13th International Conference on Applications of Statistics and Probability in Civil Engineering, ICASP13
Seoul, South Korea, May 26-30, 2019

Risk-Adaptive Learning of Seismic Response using Multi-Fidelity Analysis

Johannes O. Royset
Professor, Operations Research Dept., Naval Postgraduate School, Monterey, USA

Selim Günay
Project Scientist, Dept. of Civil and Environmental Engineering, Univ. of California, Berkeley, USA

Khalid M. Mosalam
Taisei Professor and PEER Director, Dept. of Civil and Environmental Engineering, Univ. of California, Berkeley, USA

ABSTRACT: Performance-based earthquake engineering often requires a large number of sophisticated nonlinear time-history analyses and is therefore demanding both with regard to computing resources and technical expertise. We develop a risk-adaptive statistical learning method based on multi-fidelity analysis that enables engineers to conservatively predict structural response using only low-fidelity analyses such as Pushover analyses. Using a structural model of a 35-story building in California and a training data set consisting of nonlinear time-history and pushover analyses for 160 ground motions, we accurately and conservatively predict maximum story drift ratio, top-story drift ratio, and normalized base shear under the effect of 40 ground motions not seen during the training.

1. INTRODUCTION

A main hurdle in performance-based earthquake engineering (PBEE) is the requirement to conduct a large number of nonlinear time-history (NTH) analyses with sophisticated structural models. In particular, the number of NTH analyses often becomes prohibitively large when uncertainty is treated comprehensively. These NTH analyses give rise to technical and computational issues such as lack of convergence, numerical instability, and excessive run times. An engineer with deep knowledge about and experience with NTH analysis might overcome some of these issues through tuning of algorithmic parameters and other techniques. At the present time, such skills are sometimes lacking among practicing engineers. Even if such skills become widespread, the time required to carry out algorithmic tuning and other adjustments adds significantly to the already long computing times for NTH analysis, which is often unaffordable for practitioners. Hence, there is an urgent need to reduce the number of NTH analyses required for PBEE while maintaining conservative estimates for design purposes. In this paper, we examine a risk-adaptive statistical learning method based on multi-fidelity analysis to overcome these issues.

In the presence of uncertainty, for example about structural parameters and ground motion characteristics, structural response is random, but possibly described by its mean response, standard deviation, probability of failure, and similar statistical quantities. We adopt a superquantile risk (s-risk) to describe the random response, which is defined as the average of a pre-specified fraction of the worst responses and thereby adapts to any level of risk-averseness. Rockafellar and Uryasev (2000) introduced the concept under the name conditional value-at-risk and it has been utilized widely

in finance and operations research. Rockafellar and Royset (2010) adopted the application-neutral name "superquantile," brought the concept to reliability engineering, and introduced the related notion of buffered failure probability. Decision-making theoretical background is surveyed by Rockafellar and Royset (2015a).

There are two main advantages associated with s-risk compared to the use of failure probabilities. First, it accounts for the magnitude of exceedance and thereby represents more comprehensively the resilience in a structure. Second, it can be integrated seamlessly with design optimization as laid out by Rockafellar and Royset (2010).

Still, computing s-risk of a structural response quantity of interest (QoI) using NTH analyses can be computationally costly. In this paper, we construct surrogates in terms of estimates from low-fidelity analyses that conservatively predicts a QoI. There is a large literature on surrogate models as laid out for example by Forrester et al. (2008); Freitag et al. (2014); Perdikaris et al. (2015). The distinguishing features of the present paper are its focus on estimating s-risk directly from response data and its leverage of the theoretical results by Rockafellar and Royset (2015b) to provide guarantees that the surrogates are conservative. We demonstrate the framework by investigating a structural model of a 35-story building in California under seismic load with Pushover (PO) analysis providing low-fidelity estimates.

2. SUPERQUANTILE RISK

Suppose that Y is a random variable describing a QoI, say maximum story drift ratio. Without loss of generality, we assume that low values of Y are preferred to higher values so that overestimation becomes conservative. If a practical situation demands high values, we simply replace Y by $-Y$. S-risk reduces a random variable to a representative number that can be used in comparison with requirements and design alternatives. Specifically, for risk-parameter $\alpha \in [0,1]$, the *superquantile risk* (*s-risk*) of Y, denoted by $R_\alpha(Y)$, is the

average of Y in the worst $(1-\alpha)100\%$ outcomes.

If the risk-parameter $\alpha = 0$, then $R_\alpha(Y)$ is simply the expected value $\mathbb{E}[Y]$. If $\alpha = 1$, then $R_\alpha(Y)$ is the largest possible value of Y. A value of α between these two extremes provides a middle ground. Figure 1 illustrates a situation when Y has a triangular probability density function (pdf). In this case, the worst $(1-\alpha)100\%$ outcomes are those with values greater than $1-2\sqrt{1-\alpha}$. The average across these is $R_\alpha(Y) = 1-(4/3)\sqrt{1-\alpha}$.

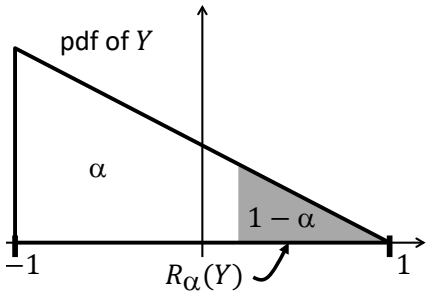

Figure 1: S-risk $R_\alpha(Y)$ is the average of the worst $(1-\alpha)100\%$ outcomes (shaded).

If the random variable Y is normal with mean μ and standard deviation σ, then $R_\alpha(Y) = \mu + \sigma\phi(\Phi^{-1}(\alpha))/(1-\alpha)$, where ϕ is the standard normal pdf and Φ is the standard normal cumulative distribution function. Generally,

$$R_\alpha(Y) = \text{minimum of } c + \mathbb{E}[\max\{0, Y-c\}]/(1-\alpha)$$

across all scalars c, which can be taken as the definition and avoids ambiguities about the meaning of "average" when there is a probability atom at the α-quantile of Y. Rockafellar and Royset (2015a) elaborate on these details.

If Y follows a discrete distribution with realizations $y_1 < y_2 < \ldots < y_m$ and corresponding probabilities $p_1, p_2, \ldots, p_m$, then

$$R_\alpha(Y) = \frac{1}{1-\alpha}\left[\left(\left(\sum_{i=1}^{j} p_i\right) - \alpha\right) y_j + \sum_{i=j+1}^{m} p_i y_i\right]$$

when $\sum_{i=1}^{j-1} p_i < \alpha \le \sum_{i=1}^{j} p_i$. If $\alpha > 1 - p_m$, then $R_\alpha(Y) = y_m$ and $R_0(Y) = \sum_{i=1}^{m} p_i y_i$. We stress that the values of Y need to be sorted.

We observe that having $R_\alpha(Y) \le r$ for some threshold r means that even on average over a set

of worst outcomes, the value of the QoI will not exceed r. The specific definition of "worst outcomes" depends on α. We can also interpret the condition probabilistically as done by Rockafellar and Royset (2010): $R_\alpha(Y) \leq r$ is equivalent to having the *buffered failure probability* $\leq 1-\alpha$ and it implies that $\text{prob}(Y > 0) \leq 1-\alpha$.

It is clear that the value of α needs to reflect the concerns of an application. The relation to the failure probability provides general guidance: If there is a need for a reliability level corresponding to a failure probability of 10^{-3}, then $\alpha = 1-10^{-3}$ achieves this goal. Since s-risk is continuous in α, small changes in α implies small changes in the s-risk, which partially alleviates the need to select α "correctly."

3. RISK-ADAPTIVE ESTIMATION

The formulas for computing $R_\alpha(Y)$ require the probability distribution of Y, which is generally not available for QoIs in structural engineering. In this section, we build on Rockafellar and Royset (2015b) to construct surrogates that conservatively approximate $R_\alpha(Y)$. Specifically, given an n-dimensional random vector $\mathbf{X}$ representing n different types of low-fidelity estimates of Y, we seek a function $h : \mathbb{R}^n \to \mathbb{R}$ such that $R_\alpha(Y) \leq R_\alpha(h(\mathbf{X}))$. In a specific sense, we obtain the lowest such upper bound as described by Rockafellar and Royset (2015b). For simplicity, we let $h(\mathbf{x}) = c_0 + \mathbf{c}^\top \mathbf{x}$, i.e., h is affine. The task then reduces to finding the coefficients c_0 and $\mathbf{c} = (c_1, c_2, \ldots, c_n)^\top$. Royset et al. (2017) and Bonfiglio et al. (2018) mirror this general direction, but concentrate on design optimization in the context of naval architecture.

We compute the coefficients as follows:

Algorithm for Risk-Adaptive Learning

1. Minimize $\mathbf{c}^\top \mathbb{E}[\mathbf{X}] + R_\alpha(Y - \mathbf{c}^\top \mathbf{X}) + \lambda \|\mathbf{c}\|_1$ and obtain an optimal $\hat{\mathbf{c}}$.
2. Set $\hat{c}_0 = R_\alpha(Y - \hat{\mathbf{c}}^\top \mathbf{X})$.

Corollary 4.2 by Rockafellar and Royset (2015b) establishes that the output $(\hat{c}_0, \hat{\mathbf{c}})$ of the algorithm satisfies

$$R_\alpha(Y) \leq R_\alpha\big(\hat{c}_0 + \hat{\mathbf{c}}^\top \mathbf{X}\big)$$

and thus furnishes a conservative surrogate for the QoI.

Step 1 of the algorithm requires us to solve a convex optimization problem in n variables, which can be achieved quickly using standard tools. Here, $\|\mathbf{c}\|_1 = \sum_{j=1}^n |c_j|$ and $\lambda \geq 0$ is a parameter that can be used to adjust the sparsity of the resulting surrogate. If λ is high, then $\hat{\mathbf{c}}$ tends to have many zero elements. Empirical evidence indicates that a choice of $\lambda > 0$ often improves estimates too.

Step 2 involves computing the s-risk of a random variable, which is obtained using the formulas of the previous section. In both steps, we need to know the joint probability distribution of $(\mathbf{X}, Y)$. Since the actual distribution may not be known, we use a training data set consisting of a number of observations of these random variables. We note that the size of the optimization problem in Step 1 is independent of the amount of training data and thus is scalable.

Since the algorithm is carried out on a training data set, and not using the actual distribution, the resulting surrogate is only guaranteed to be conservative with respect to the (empirical) distribution induced by this training data set. To obtain robust predictions beyond the training data set (generalization), we implement a cross-validation approach. We refer to Meckesheimer et al. (2002); Goel et al. (2009); Viana et al. (2009); Zhang et al. (2014); Mehmani et al. (2015) for the use of cross-validation in surrogate models broadly. We simply apply the algorithm repeatedly, say m times, using randomly selected data from the training data set and obtain a collection of coefficients $\{\hat{c}_0^i, \hat{\mathbf{c}}^i,\ i = 1, \ldots, m\}$. Each pair $(\hat{c}_0^i, \hat{\mathbf{c}}^i)$ furnishes a prediction. The variation across the predictions quantifies estimation uncertainty and allows us to give confidence intervals as described below.

4. NUMERICAL EXAMPLE

To illustrate the framework we consider a case study from earthquake engineering.

4.1. Structural Model

We study a 35-story building described in Mahin et al. (2015) under 200 different ground motions

and record three QoIs: (1) maximum story drift ratio (max story drift / story height), (2) top-story drift ratio (top-story displacement / building height), and (3) normalized base shear (base shear / weight). The building has an approximate height of 490-ft with a typical story height of 13-ft and plan dimensions of 185-ft by 135-ft. The structural system of the building is comprised of complete steel moment-resisting space frames with welded connections. The steel frames primarily consist of built-up box (single-cell or two-cell) or wide flange columns welded to beams (either built-up or hot-rolled sections). A typical 6-in.-thick concrete slab on metal deck exists at each floor. The foundation of the building consists of a 7-ft thick mat located 40-ft below grade and supported by more than 2,500 concrete piles that extending to 60-ft below the mat. The foundation mat is connected to a 3-ft thick retaining wall running around the entire foundation. Beam-to-column moment connections incorporate typical pre-Northridge details. Column splices are made of relatively brittle partial joint penetration welds located about 4 ft. from the lower floor level. A perspective view of the building is shown in Figure 2(a).

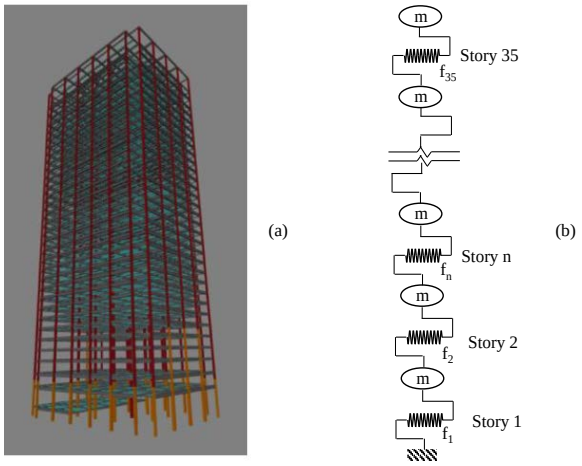

Figure 2: (a) Perspective view of the 35-story building; (b) structural model used in NTH analyses.

For the purposes of this study, we develop in OpenSees, McKenna (2010), a simplified model of the building using spring elements that represent the story force-displacement relationships; see Figure 2(b). The material Steel01 in OpenSees is used to define these relationships with parameters given in Figure 3. The values of the parameters that define these force-displacement relations, namely V_y, k, and α, are based on the PO and eigenvalue analyses conducted in Mahin et al. (2015). The first four mode periods of the building are 4.18 sec, 1.40 sec, 0.84 sec, and 0.60 sec. Two hundred ground motions are considered that match the target spectral acceleration at the first mode period for 5% damping, which is determined as 0.26g for the location of the building in Northern California. One NTH and one PO analyses take 55 and 12 seconds on a single core, respectively. In practice, NTH analysis would take much longer; the numerical results are meant to simply illustrate the approach.

The NTH analysis are conducted using Explicit Newmark integration to avoid convergence problems as discussed by Liang et al. (2016). The resulting responses are considered "high-fidelity" in the present study. PO analyses per ASCE41-13 (American Society of Civil Engineers (2014)) furnish "low-fidelity" estimates.

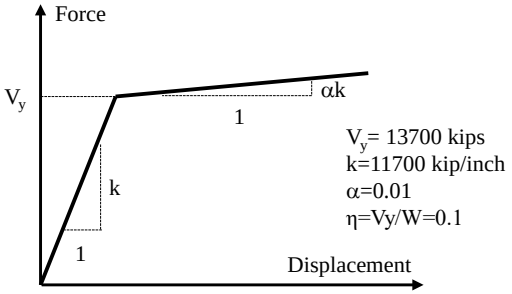

Figure 3: Story force-displacement relationship.

4.2. Numerical Results

For each of the 200 ground motions, we carry out NTH and PO analyses to obtain responses for the three QoIs. The resulting data set is divided in two parts. The first part corresponding to 160 ground motions forms the training data set and the second part of 40 ground motions forms a test data set on which we will check the accuracy of the computed surrogates.

A preliminary examination of the full data set gives an indication of the difficulty that we face. Figure 4 shows low- and high-fidelity responses for QoI 1 (maximum story drift ratio) across the 200

ground motions. It is immediately clear that a naive linear least-squares regression model between the two kinds of responses would not be informative; knowledge about a low-fidelity response does not seem to point strongly to a corresponding high-fidelity response. The situation is similar for QoI 2 (top-story drift ratio), Figure 5, and even worse for QoI 3 (normalized base shear), Figure 6. Despite this situation, we see below that informative surrogates can be developed.

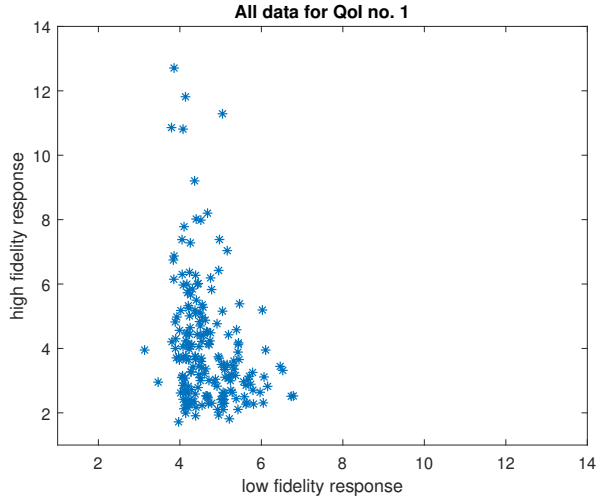

Figure 4: QoI 1 across 200 ground motions by low-fidelity (PO) and high-fidelity (NTH) analyses.

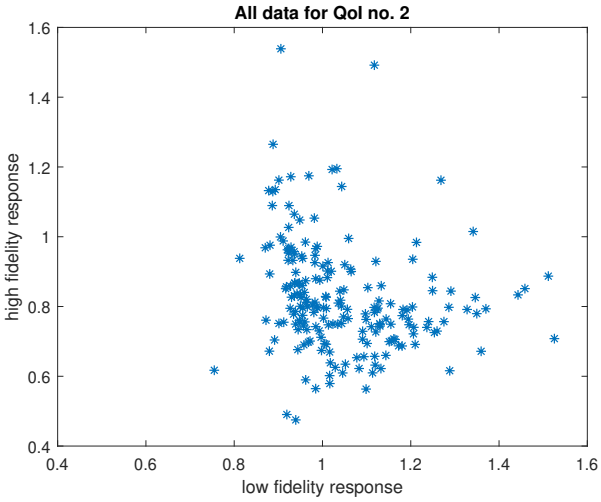

Figure 5: QoI 2 across 200 ground motions by low-fidelity (PO) and high-fidelity (NTH) analyses.

We proceed with the procedure of Section 3 with $\alpha = 0.9$, i.e., we aim to estimate (conservatively)

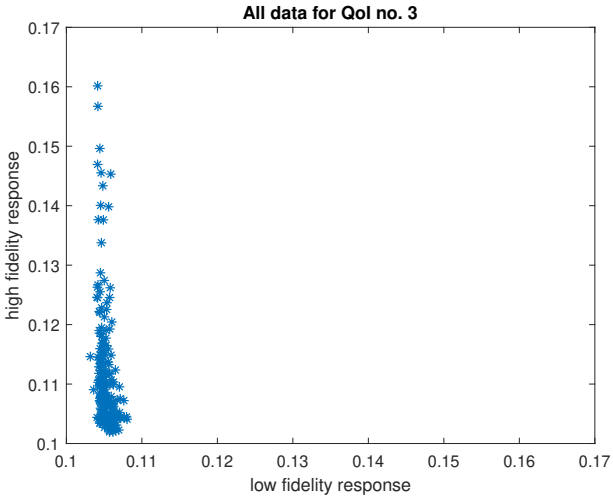

Figure 6: QoI 3 across 200 ground motions by low-fidelity (PO) and high-fidelity (NTH) analyses.

the average of the worst 10% responses. The regularization parameter $\lambda = 0.00001$ is assumed, with further improvement of the below results being possible by systematically optimizing this parameter. Although the framework permits any number, we have only one type of low-fidelity analyses. Still, we artificially create a second one by taking the square of the low-fidelity responses, i.e., $\mathbf{X} = (X, X^2)$, with X being the random variable corresponding to the low-fidelity responses. Thus, we seek to determine the coefficients c_0, c_1, c_2 in the model

$$c_0 + c_1 X + c_2 X^2.$$

The risk-adaptive learning algorithm is run 20 times for every QoI, each time using 100 randomly selected data points (with replacement) from the training data set corresponding to 160 ground motions. In total, the 20 times 3 runs of the learning algorithm take less than 30 seconds on a standard laptop. Figure 7 shows the resulting 20 curves in the case of QoI, each one furnishes a prediction of high-fidelity response given any value of the low-fidelity response. Although each one of the curves are conservative with respect to the underlying training data set, as guaranteed by the supporting theory, it may not be conservative with respect to the test data set of responses to 40 ground motions not used during the training and illustrated in the figure with "*." As described in Section

3, the 20 curves offer the possibility of constructing confidence intervals. To be consistent with the framework, we construct confidence intervals not using mean and standard deviations, but rather superquantiles. Specifically, let $\{\hat{c}_0^i, \hat{\mathbf{c}}^i,\ i = 1,\ldots,20\}$ denote the coefficients of the 20 curves in Figure 7 and $\{x_j, y_j, j = 1,\ldots,40\}$ be the low- and high-fidelity responses for QoI 1 in the test data set. The mean of $\{\hat{c}_0^i + \hat{c}_1^i x_j + \hat{c}_2^i x_j^2,\ i = 1,\ldots,20\}$, i.e., the average of the values of the curves at x_j furnishes the lower end of the confidence interval and the β-superquantile of $\{\hat{c}_0^i + \hat{c}_1^i x_j + \hat{c}_2^i x_j^2,\ i = 1,\ldots,20\}$, i.e., the average of the worst $(1-\beta)\%$ outcomes gives the upper end of the confidence interval. We note that this confidence interval does not aim to estimate y_j but rather an upper bound on y_j. Using $\beta = 0.8$, Figure 8 illustrates these confidence intervals with black lines for all $j = 1,\ldots,40$ and also depicts y_j with "*." The figure shows that for all the 40 test data points the upper end of the confidence interval is indeed an upper bound on y_j. In 39 cases, the lower end is also an upper bound on y_j. The confidence intervals are mostly quite conservative, but this is expected in view of the poor correlation seen in Figure 4.

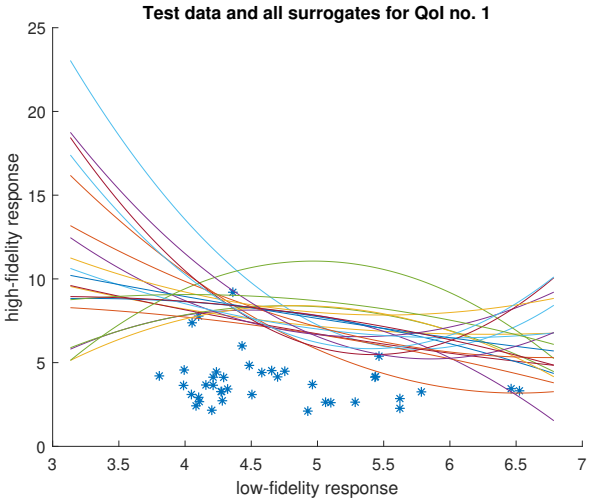

Figure 7: Surrogates and test data for QoI 1.

The situation is similar for QoI 2, but sometimes the level of conservativeness is less than for QoI 1; see Figures 9 and 10. (The high confidence interval at test data 18 is explained by a somewhat "unlucky" draw of training data, but it still furnishes an upper bound on y_j as desired.

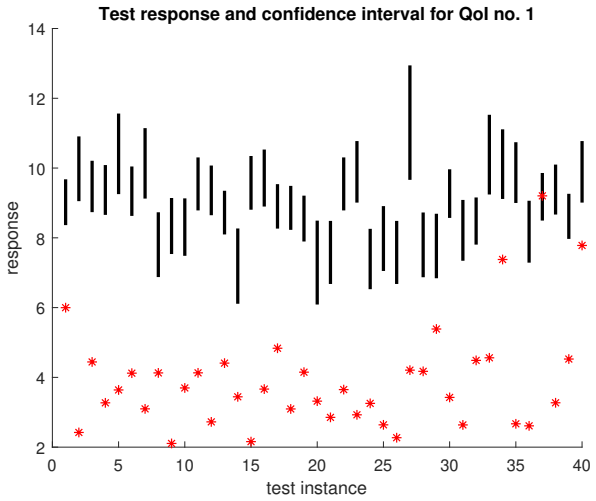

Figure 8: Confidence intervals for QoI 1.

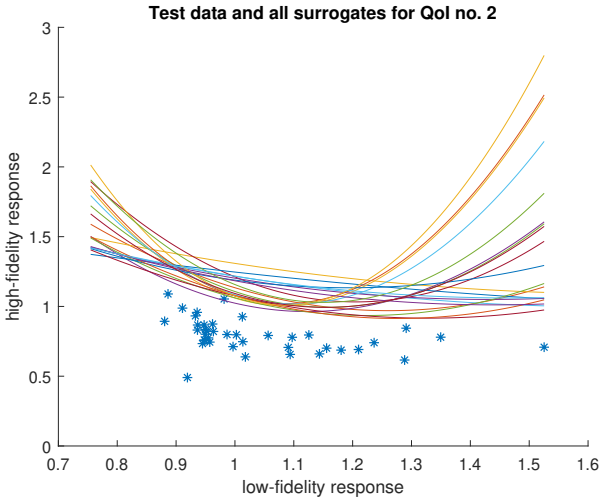

Figure 9: Surrogates and test data for QoI 2.

In the case of QoI 3, which represents the largest challenge in view of Figure 6, we see from Figures 11 and 12 that indeed it becomes especially important to consider more than one surrogate; sometimes only the upper end of the confidence interval is an upper bound on y_j. There are even two test data points where y_j even exceeds the upper end. Statistically, this is expected in view of our choice of $\beta = 0.8$, with a higher value making such events less likely. We still find the confidence intervals to provide useful estimates of y_j even in this difficulty case of nearly no correlation between high- and low-fidelity analyses.

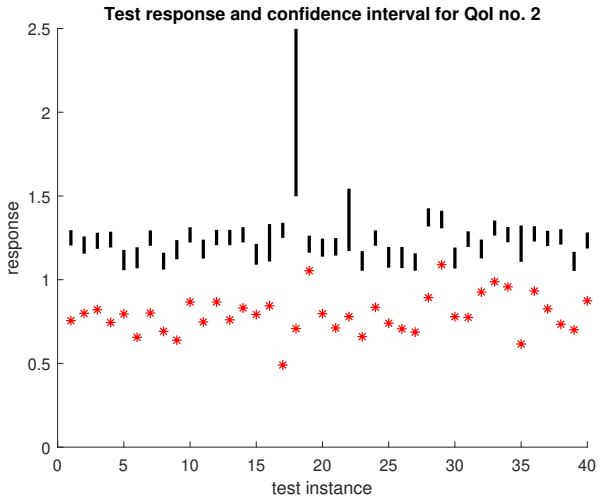

Figure 10: Confidence intervals for QoI 2.

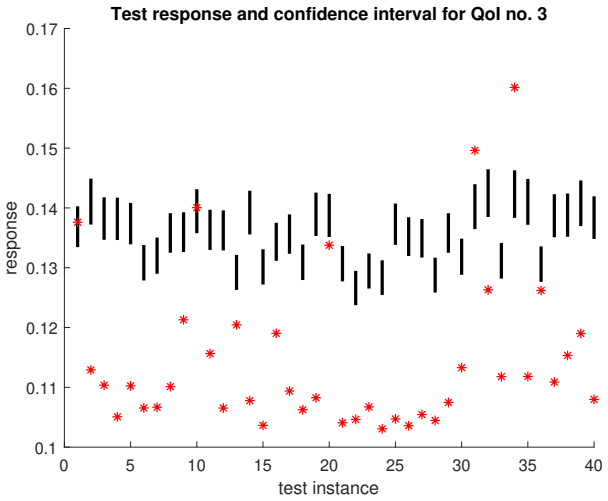

Figure 12: Confidence intervals for QoI 3.

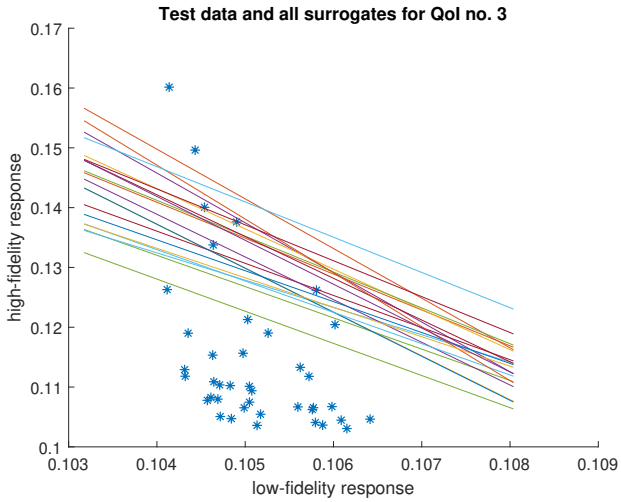

Figure 11: Surrogates and test data for QoI 3.

An interesting effect is present for all three QoIs and that is especially prominent in Figure 11: higher values of the low-fidelity response are predicted to correspond to *lower* values of the high-fidelity response. The curves in Figure 11 have negative slopes. At first this may appear counter intuitive. However, since lower low-fidelity responses tend to have larger errors than higher low-fidelity responses, and our predictions need to account for this uncertainty, risk-adaptive predictions naturally have this characteristic.

Table 1 aggregates these predictions across the test data set. The second column provides the actual s-risk of the QoI, i.e., $R_\alpha(Y)$, where Y is

Table 1: Confidence intervals for bound on s-risk.

	actual s-risk	predicted upper bound
QoI 1	7.59	[9.32, 11.79]
QoI 2	1.02	[1.35, 1.72]
QoI 3	0.147	[0.138, 0.146]

distributed according to the high-fidelity responses $\{y_j, j = 1,\ldots,40\}$ in the test set. The third column gives $R_\beta(R_\alpha(\hat{c}_0^i + \hat{c}_1^i x_j + \hat{c}_2^i x_j^2, j = 1,\ldots,40), i = 1,\ldots,20)$, i.e., first the α-superquantile of $\{\hat{c}_0^i + \hat{c}_1^i x_j + \hat{c}_2^i x_j^2, j = 1,\ldots,40\}$ is computed for each i and then the β-superquantile is computed across i. The lower end of the confidence intervals in the table are provided by $\beta = 0$ and the upper end by $\beta = 0.8$. The table provides an empirical indication that the guaranteed property $R_\alpha(Y) \leq R_\alpha(\hat{c}_0 + \hat{\mathbf{c}}^\top \mathbf{X})$ for the training data generalizes to the test data when "robustified" by considering 20 surrogates.

5. CONCLUSIONS

The paper establishes that risk-adaptive statistical learning provides a promising approach to generating conservative estimates of responses in nonlinear time-history analyses using only pushover analyses. The approach provides accurate or conservative estimates of three quantities under the effect of 40 ground motions not seen during statistical training. These accomplishments are especially interesting in view of the fact that no strong correlation between the analysis types can

be detected in the training data. We are therefore hopeful that risk-adaptive statistical learning of the kind laid out in this paper can offer an efficient and simple approach to response prediction using only low-fidelity simulations. This is expected to be of significant value in rapid assessment on a regional scale in the aftermath of a major extreme event.

Acknowledgement. The authors thank Jaewon Saw and Fan Hu for assisting with simulations.

6. REFERENCES

American Society of Civil Engineers (2014). "Seismic evaluation and retrofit of existing buildings (ASCE/SEI 41-13)." *ASCE, Reston, VA*.

Bonfiglio, L., Royset, J. O., and Karniadakis, G. (2018). "Multi-disciplinary risk-adaptive design of supercavitating hydrofoils." *AIAA Non-Deterministic Approaches Conference, AIAA SciTech Forum, (AIAA 2018-1177)*.

Forrester, A., Sobester, A., and Keane, A. (2008). *Engineering Design via Surrogate Modelling: A Practical Guide*. Wiley.

Freitag, S., Cao, B. T., Ninic, J., and Meschke, G. (2014). "Surrogate modeling for mechanized tunneling simulations with uncertain data." *Proceedings of the 6th International Workshop on Reliable Engineering Computing (REC 2014), Chicago*, 44–63.

Goel, T., Haftka, R. T., and Shyy, W. (2009). "Comparing error estimation measures for polynomial and kriging approximation of noise-free functions." *Structural and Multidisciplinary Optimization*, 38(5), 429–442.

Liang, X., Mosalam, K. M., and Günay, S. (2016). "Direct integration algorithms for efficient nonlinear seismic response of reinforced concrete highway bridges." *Journal of Bridge Engineering*, 04016041.

Mahin, S., Lai, J. W., S, S. W., and Schoettler, M. (2015). "Evaluating and improving the seismic performance of older tall buildings." *Second International Conference on Performance-based and Life-cycle Structural Engineering (PLSE 2015), Dec. 9-11, Brisbane, Australia*.

McKenna, F. (2010). "Opensees user's manual." *http://opensees.berkeley.edu*.

Meckesheimer, M., Booker, A. J., Barton, R. R., and Simpson, T. W. (2002). "Computationally inexpensive metamodel assessment strategies." *AIAA J.*, 40(10), 2053–2060.

Mehmani, A., Chowdhury, S., and Messac, A. (2015). "Predictive quantification of surrogate model fidelity based on modal variations with sample density." *Structural and Multidisciplinary Optimization*, 52(2), 353–373.

Perdikaris, P., Venturi, D., Royset, J. O., and Karniadakis, G. (2015). "Multi-fidelity modeling via recursive co-kriging and gaussian markov random fields." *Royal Society Proceedings A*, 2179(471).

Rockafellar, R. T. and Royset, J. O. (2010). "On buffered failure probability in design and optimization of structures." *Reliability Engineering & System Safety*, 95, 499–510.

Rockafellar, R. T. and Royset, J. O. (2015a). "Engineering decisions under risk-averseness." *ASCE-ASME J. Risk and Uncertainty in Engineering Systems, Part A: Civil Engineering*, 1(2), 04015003.

Rockafellar, R. T. and Royset, J. O. (2015b). "Measures of residual risk with connections to regression, risk tracking, surrogate models, and ambiguity." *SIAM J. Optimization*, 25(2), 1179—1208.

Rockafellar, R. T. and Uryasev, S. (2000). "Optimization of conditional Value-at-Risk." *Journal of Risk*, 2, 493–517.

Royset, J. O., Bonfiglio, L., Vernengo, G., and Brizzolara, S. (2017). "Risk-adaptive set-based design and applications to shaping a hydrofoil." *ASME J. Mechanical Design*, 139(10), 1014031–1014038.

Viana, F. A. C., Haftka, R. T., and Steffen, V. (2009). "Multiple surrogates: How cross-validation errors can help us to obtain the best predictor." *Structural and Multidisciplinary Optimization*, 39(4), 439–457.

Zhang, J., Chowdhury, S., Mehmani, A., and Messac, A. (2014). "Characterizing uncertainty attributable to surrogate models." *ASME J. Mechancial Design*, 136(3), 031004.